Biochemistry

pubs.acs.org/biochemistry Article

Why Are Lopinavir and Ritonavir Effective against the Newly Emerged Coronavirus 2019? Atomistic Insights into the Inhibitory Mechanisms

Bodee Nutho,[⊥] Panupong Mahalapbutr,[⊥] Kowit Hengphasatporn, Nawanwat Chainuwong Pattaranggoon, Nattapon Simanon, Yasuteru Shigeta, Supot Hannongbua,* and Thanyada Rungrotmongkol*

Cite This: https://dx.doi.org/10.1021/acs.biochem.0c00160 Read Online

ACCESS | Metrics & More | Article Recommendations | Supporting Information

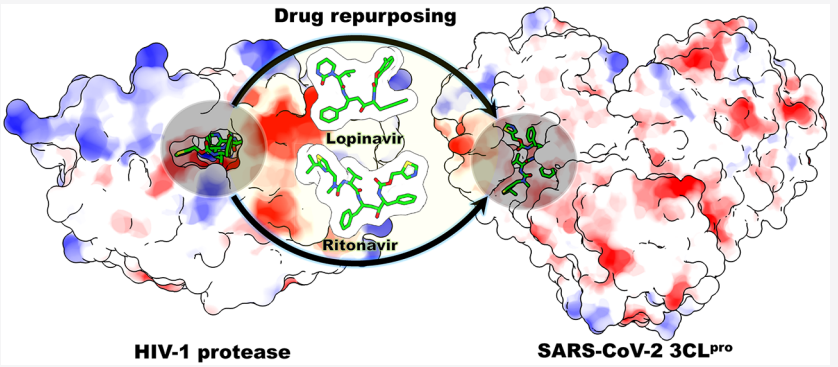

ABSTRACT: Since the emergence of a novel coronavirus disease 2019 (COVID-19) caused by severe acute respiratory syndrome coronavirus 2 (SARS-CoV-2) was first reported from Wuhan, China, neither a specific vaccine nor an antiviral drug against SARS-CoV-2 has become available. However, a combination of two HIV-1 protease inhibitors, lopinavir and ritonavir, has been found to be effective against SARS-CoV, and both drugs could bind well to the SARS-CoV 3C-like protease (SARS-CoV 3CL^{pro}). In this work, molecular complexation between each inhibitor and SARS-CoV-2 3CL^{pro} was studied using all-atom molecular dynamics simulations, free energy calculations, and pair interaction energy analyses based on MM/PB(GB)SA and FMO-MP2/PCM/6-31G* methods. Both anti-HIV drugs interacted well with the residues at the active site of SARS-CoV-2 3CL^{pro}. Ritonavir showed a somewhat higher number atomic contacts, a somewhat higher binding efficiency, and a somewhat higher number of key binding residues compared to lopinavir, which correspond with the slightly lower water accessibility at the 3CL^{pro} active site. In addition, only ritonavir could interact with the oxyanion hole residues N142 and G143 via the formation of two hydrogen bonds. The interactions in terms of electrostatics, dispersion, and charge transfer played an important role in the drug binding. The obtained results demonstrated how repurposed anti-HIV drugs could be used to combat COVID-19.

In December 2019, there were many cases of patients reported to have a respiratory tract infection with severe pneumonia in Wuhan, China. It was found that these patients most likely had an epidemiological history related to a seafood market in that area of China.[1] However, a newly causative microbial infection cannot at first be identified in public databases. On the basis of whole genome sequencing, it was revealed that this microbial pathogen is a novel coronavirus, formally named 2019-nCoV, closely related to the bat severe acute respiratory syndrome (SARS)-like coronavirus, so-called SARS-CoV-2.[2,3] The World Health Organization (WHO) has officially confirmed the outbreak of 2019-nCoV on December 31, 2019, and eventually officially named it coronavirus disease 2019 or COVID-19. In general, coronaviruses are characterized as enveloped, positive-sense, single-stranded RNA viruses in the genus *Coronavirus* of the family Coronaviridae and can infect humans and several animals, including mammals and birds.[4−7] Nonetheless, some coronaviruses can potentially cause severe infection in patients such as the well-known outbreak of SARS-CoV in Guangdong, China,[8] and Middle East respiratory syndrome coronavirus (MERS-CoV) in many countries of the Middle East.[9] Likewise, COVID-19 has been confirmed to be transmitted from humans

Received: February 26, 2020
Revised: April 8, 2020
Published: April 15, 2020

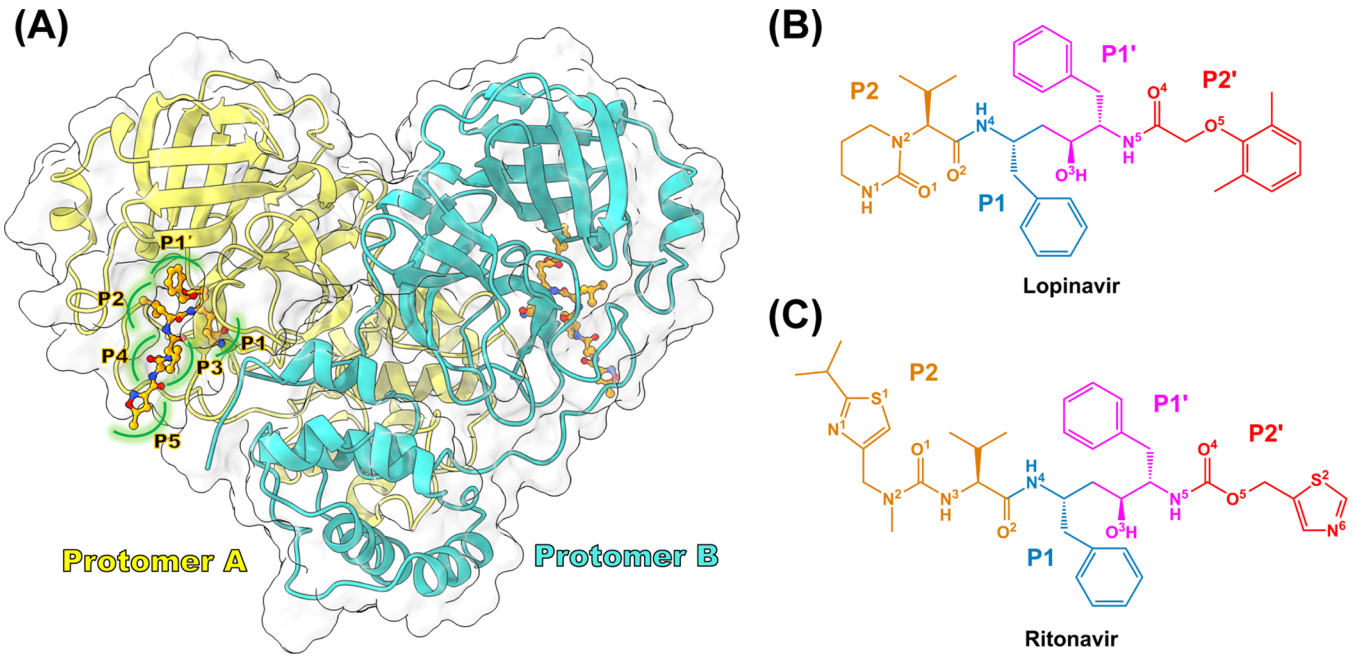

Figure 1. (A) Three-dimensional structure of the peptidelike inhibitor binding to the active site of the SARS-CoV-2 3CL^{pro} homodimer (PDB entry 6LU7) in one asymmetric unit (A, yellow; B, cyan). Protomers are shown as ribbons, and the inhibitor is shown as an orange ball and stick model. Chemical structures of (B) lopinavir and (C) ritonavir, where the atomic labels are also given.

to humans and quickly spread in several countries throughout the world.[10]

SARS-CoV-2 is a betacoronavirus, like SARS-CoV and MERS-CoV, both of which have their origins in bats.[11] For the clinical symptoms, COVID-19 infection culminates in fatal pneumonia with the clinical presentation greatly resembling SARS-CoV infection.[1] Patients infected with SARS-CoV-2 might also develop acute respiratory distress syndrome, leading to a high rate of admission to intensive care units and ultimately death in severe cases.[7] After infection, patients presented mild to severe symptoms, including fever, cough, sore throat, rhinorrhea, severe pneumonia, and septic shock.[1,7]

To date, many companies and academic research groups around the world have focused on searching for and developing a specific vaccine or antiviral drug to prevent or control emerging SARS-CoV-2 infections (e.g., vaccine, monoclonal antibodies, and small-molecule drugs). However, these options need several months to years for their development. Because of the urgent need to alleviate the COVID-19 pandemic, the use of repurposed existing antiviral drugs approved for treatment of other viral infections such as human immunodeficiency virus (HIV), hepatitis B virus, hepatitis C virus, and influenza is somewhat promising,[12] based on previous successes of the therapeutic treatment with two relevant human coronaviruses, SARS-CoV and MERS-CoV. According to numerous previous studies,[1,7,13−16] the nonstructural protein of coronavirus, in particular, main proteases or 3C-like proteases (3CL^{pro}), is considered an attractive drug target for the treatment of coronavirus infection. The role of this protease involves the proteolytic processing of the replicase polyprotein and is crucial for viral replication and maturation.[17] Moreover, 3CL^{pro} has a similar common cleavage site among coronaviruses.[18] The sequence alignment of SARS-CoV-2 3CL^{pro} (see Figure S1) shows that the SARS-CoV-2 proteinase is highly conserved compared to that of SARS-CoV with a 96.1% sequence identity.

A combination of the two approved drugs for HIV infection, lopinavir and ritonavir (KALETRA), has been reported to be active toward SARS and MERS.[14,19] Both anti-HIV drugs were initially purposed to inhibit 3CL^{pro} of SARS-CoV and MERS-CoV, and they appeared to be related to clinical benefits of patients with SARS in a nonrandomized open-label trial.[17] Although ritonavir is a protease inhibitor, it is generally used to inhibit cytochrome P450 3A4 and markedly increases the plasma concentrations of other protease inhibitors.[20] Nevertheless, whether HIV protease inhibitors could effectively target SARS-CoV-2 3CL^{pro} is under debate. This is based on the fact that HIV protease is from the aspartic protease family, whereas SARS-CoV-2 3CL^{pro} belongs to the cysteine protease family. Previously, a theoretical study of the molecular interaction of lopinavir and ritonavir with 3CL^{pro} of SARS-CoV suggested that these two drugs could bind well at the substrate-binding pocket of SARS-CoV 3CL^{pro}.[15] To date, the three-dimensional structure of SARS-CoV-2 3CL^{pro} in a complex with lopinavir and ritonavir has not been reported. Thus, in our study, we aimed to investigate the binding interactions of lopinavir and ritonavir with the SARS-CoV-2 proteinase using both molecular modeling and quantum chemical methods. It is our hope that this information can be useful for the future design or development of more specific inhibitors for the treatment of human coronaviruses.

COMPUTATIONAL DETAILS

System Preparation. The co-crystal structure of homodimeric SARS-CoV-2 3CL^{pro} in complex with a peptidomimetic inhibitor [*N*-[(5-methylisoxazol-3-yl)carbonyl]alanyl-L-valyl-*n*-1-((1*R*,2*Z*)-4-(benzyloxy)-4-oxo-1-{[(3*R*)-2-oxopyrrolidin-3-yl]methyl}but-2-enyl)-L-leucinamide] was retrieved from the RSCB Protein Data Bank (PDB entry 6LU7).[21] Note that each moiety of the peptidomimetic inhibitor is associated with the -P5-P4-P3-P2-P1-P1′- positions of the 3CL^{pro} cleavage site (Figure 1A). To generate the models of SARS-CoV-2 3CL^{pro}

https://dx.doi.org/10.1021/acs.biochem.0c00160
Biochemistry XXXX, XXX, XXX−XXX

with lopinavir and ritonavir bound to protomer A, the positions of the original peptidelike inhibitor were changed to the corresponding drug for each P position (Figure 1B,C). This modification was performed according to the similar orientation with the template inhibitor using the small molecules tool implemented in Accelrys Discovery Studio 2.5 (Accelrys Inc.). The protonation states of all ionizable amino acids were assigned at pH 7.4 using the H++ web server,[22] except for the catalytic residue H41 that was set as the neutral form with a protonated delta position (HID type of AMBER format) in accordance with the common reaction mechanism of cysteine protease.[23] The chemical structures of lopinavir (ZINC3951740) and ritonavir (ZINC3944422) were downloaded from the ZINC15 database.[24] The electrostatic potential (ESP) charges of both ligands were calculated with the HF/6-31G* level of theory using the Gaussian09 program.[25] The antechamber and parmchk modules of AMBER16 were used to generate the restrained ESP charges and missing parameters of the two drugs, respectively. The bonded and nonbonded parameters for the protein and ligand were treated with the AMBER ff14SB force field[26] and generalized AMBER force field version 2 (GAFF2),[27] accordingly. Missing hydrogen atoms were added using the LEaP module implemented in AMBER16. Afterward, the TIP3P water model[28] was used to solvate each system with a minimum distance of 10 Å between the protein surface and the solvation box edge, and the box dimensions were set to approximately 114 Å × 97 Å × 92 Å. The sodium ions were then randomly added to neutralize the simulated systems. The added hydrogen atoms and water molecules were minimized using 500 steps of steepest descent (SD) followed by 1500 steps of conjugated gradient (CG) methods before running the MD simulations, while the rest of the molecules were held fixed. Then, the protein and ligand were minimized by SD (500 iterations) and CG (1500 iterations) methods with constrained solvent molecules. Finally, the whole complex was fully minimized using the same procedure.

Molecular Dynamics Simulations. Each system was simulated under the periodic boundary condition with the isothermal−isobaric (*NPT*) scheme, as previously described.[29−32] Briefly, a cutoff distance for nonbonded interactions was set to 10 Å, while the particle mesh Ewald summation method[33] was employed to treat the electrostatic interactions. The SHAKE algorithm[34] was used to constrain all covalent bonds involving hydrogen atoms. A 2 fs simulation time step was used throughout the MD simulation. The temperature and pressure were controlled by the Langevin thermostat[35] with a collision frequency of 2 ps^{-1} and the Berendsen barostat[36] with a pressure-relaxation time of 1 ps. For the heating step, each simulated system was gradually heated from 10 to 310 K for 200 ps with a harmonic positional restraint of 30.0 kcal mol^{-1} $Å^{-2}$ applied to the Cα atoms of the protein. To equilibrate the system, each complex was then subjected to four steps of restrained MD simulations at 310 K with harmonic restraints of 30, 20, 10, and 5 kcal mol^{-1} $Å^{-2}$ for 1300 ps in total and another 200 ps without any restraint. Subsequently, the entire system was simulated under the *NPT* ensemble (310 K and 1 atm) until reaching 100 ns. The MD trajectories were saved every 10 ps. The calculations in terms of the root-mean-square displacement (RMSD), the number of protein−drug hydrogen bonds (# H-bonds), and the number of atomic contacts (# atom contacts) with the drug molecule were used to verify the stability of all investigated models as well as the structural features of each complex. The H-bond interactions were calculated using two criteria: (i) distance between the hydrogen donor (HD) and acceptor (HA) of ≤3.5 Å and (ii) HD−H···HA angle of ≥150°. The # atom contacts were counted from the number of $3CL^{pro}$ atoms within 3.5 Å of each drug. To evaluate the binding affinity and the key binding residues involved in ligand binding of the protein−ligand complexes, the total binding free energy (ΔG_{bind}) and per-residue decomposition free energy ($\Delta G_{bind}^{residue}$) calculations based on molecular mechanics/Poisson−Boltzmann (generalized Born) surface area [MM/PB(GB)SA] methods were performed on 100 MD snapshots extracted from the last 20 ns of the MD production phase. It should be noted that the protein−ligand interactions and the binding free energies were carried out using the CPPTRAJ[37] and MMPBSA.py[38] modules of AMBER16, respectively. Furthermore, the intermolecular interactions between the drug and its binding residues at the atomic level were described by pair interaction energy decomposition analysis (PIEDA) based on the fragment molecular orbital (FMO) method at the second-order Møller−Plesset perturbation energy and the 6-31G* level of theory (FMO-MP2/6-31G*) using GAMESS.[39] The solvation effect was also treated with a polarizable continuum model (PCM). The paired interaction energy (ΔE_{ij}^{PIEDA}) involved in ligand binding was evaluated by a summation of the electrostatic (E_{ij}^{ES}), dispersion (E_{ij}^{DI}), charge transfer (E_{ij}^{CT+mix}), and charge exchange (E_{ij}^{EX}) energies, as well as PCM solvation (G_{sol}^{PCM}), using the following equation:[40−42]

$$\Delta E_{ij}^{PIEDA} = \Delta E_{ij}^{ES} + \Delta E_{ij}^{DI} + \Delta E_{ij}^{CT+mix} + \Delta E_{ij}^{EX} + \Delta G_{sol}^{PCM}$$

RESULTS AND DISCUSSION

System Stability. The stability of each simulated model was determined by calculating the all-atom RMSD for the drug−

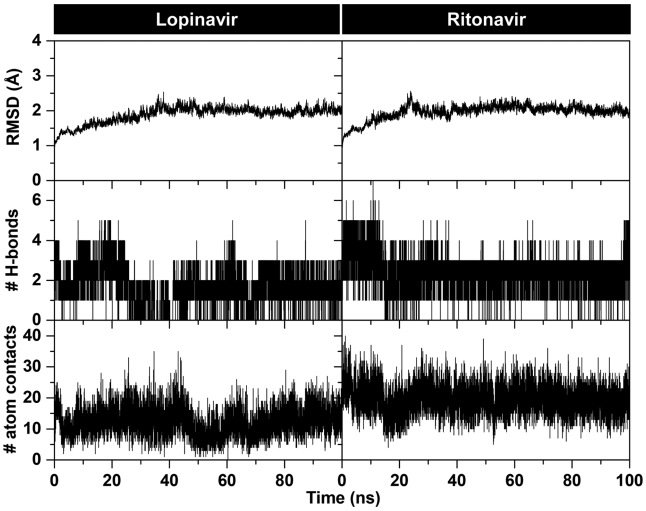

Figure 2. All-atom RMSD, # H-bonds, and # atom contacts of lopinavir (left) and ritonavir (right) in complex with SARS-CoV-2 $3CL^{pro}$ plotted along the 100 ns MD simulation.

$3CL^{pro}$ complex, the number of intermolecular H-bonds (# H-bonds), and the number of atom contacts (# atom contacts) with the drug molecule versus the simulation time. As shown in Figure 2, the RMSD values of both lopinavir and ritonavir systems continuously increased in the first 40 ns and then maintained at a fluctuation of ∼2.0 Å until the end of the

https://dx.doi.org/10.1021/acs.biochem.0c00160
Biochemistry XXXX, XXX, XXX−XXX

Table 1. ΔG_{bind} Values (kilocalories per mole) of Lopinavir and Ritonavir in Complex with SARS-CoV-2 3CL^{pro} Calculated by the MM/PB(GB)SA Method[a]

energy component	lopinavir	ritonavir
	Gas Term	
ΔE_{vdW}	−50.29 ± 0.62	−74.09 ± 0.50
ΔE_{ele}	−19.68 ± 0.50	−23.35 ± 0.56
ΔE_{MM}	−69.97 ± 0.87	−97.44 ± 0.60
$-T\Delta S$	22.47 ± 1.79	29.46 ± 1.77
	Solvation Term	
	PBSA	
$\Delta G_{sol(PBSA)}^{ele}$	41.64 ± 0.53	59.47 ± 0.46
$\Delta G_{sol(PBSA)}^{nonpolar}$	−5.03 ± 0.04	−6.42 ± 0.02
$\Delta G_{sol(PBSA)}$	36.61 ± 0.51	53.04 ± 0.45
	GBSA	
$\Delta G_{sol(GBSA)}^{ele}$	40.11 ± 0.40	48.72 ± 0.37
$\Delta G_{sol(GBSA)}^{nonpolar}$	−6.43 ± 0.07	−8.53 ± 0.04
$\Delta G_{sol(GBSA)}$	33.67 ± 0.37	40.19 ± 0.37
	Binding Free Energy	
$\Delta G_{bind(MM/PBSA)}$	−10.89 ± 1.89	−14.93 ± 1.83
$\Delta G_{bind(MM/GBSA)}$	−13.83 ± 1.91	−27.78 ± 1.82

[a]Data are shown as means ± the standard error of the mean (SEM).

simulation time, as supported by a high fluctuation of # H-bonds and # atom contacts in the first 40 ns. It should be noted that the # H-bonds and # atom contacts of the ritonavir system (# H-bonds of 3 ± 1 and # atom contacts of 19 ± 4 over the last 20 ns) were higher than those of the lopinavir model (# H-bonds of 2 ± 1 and # atom contacts of 14 ± 4), suggesting that ritonavir was more susceptible to SARS-CoV-2 3CL^{pro} (discussed in more detail below). In this work, the MD trajectories from 80 to 100 ns were thus extracted for further analysis in terms of (i) the binding affinity between lopinavir or ritonavir and SARS-CoV-2 3CL^{pro}, (ii) key binding residues involved in drug binding, (iii) protein−drug H-bonding, and (iv) water accessibility at the enzyme active site.

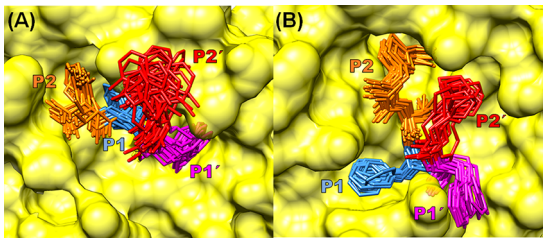

Figure 4. Superimposed structures over the 20 snapshots of (A) lopinavir and (B) ritonavir in complex with SARS-CoV-2 3CL^{pro} derived from the last 20 ns of MD simulations.

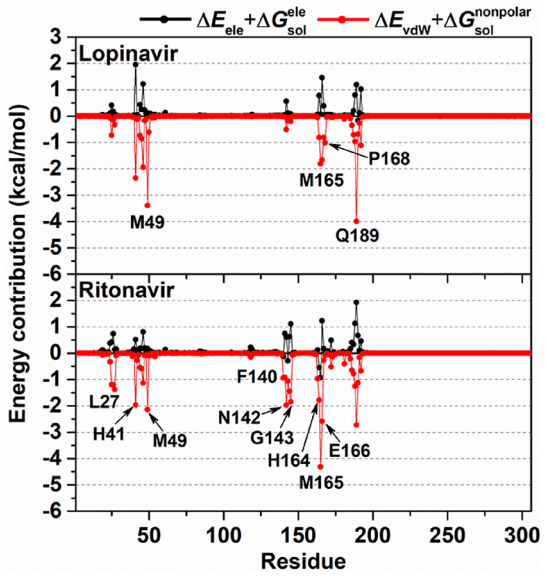

Figure 5. Electrostatic (ΔE_{ele} + ΔG_{polar}, black line) and vdW (ΔE_{vdW} + $\Delta G_{nonpolar}$, red line) energy contributions from each residue of SARS-CoV-2 3CL^{pro} to the binding of lopinavir (top) and ritonavir (bottom).

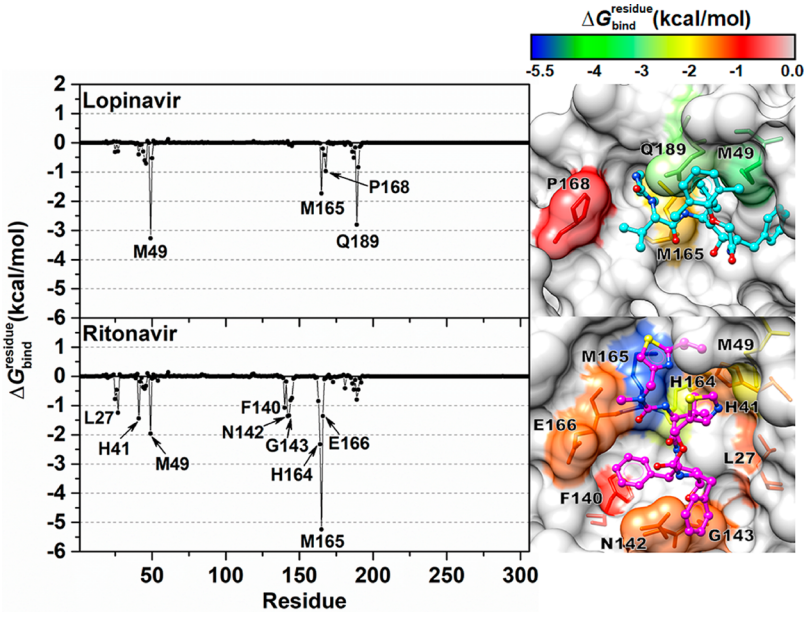

Figure 3. $\Delta G_{bind}^{residue}$ values of lopinavir (top) and ritonavir (bottom) in complex with SARS-CoV-2 3CL^{pro}. The contributing residues involved in ligand binding are colored according to their $\Delta G_{bind}^{residue}$ values, where the highest to lowest free energies are shaded from gray to blue, respectively.

https://dx.doi.org/10.1021/acs.biochem.0c00160
Biochemistry XXXX, XXX, XXX−XXX

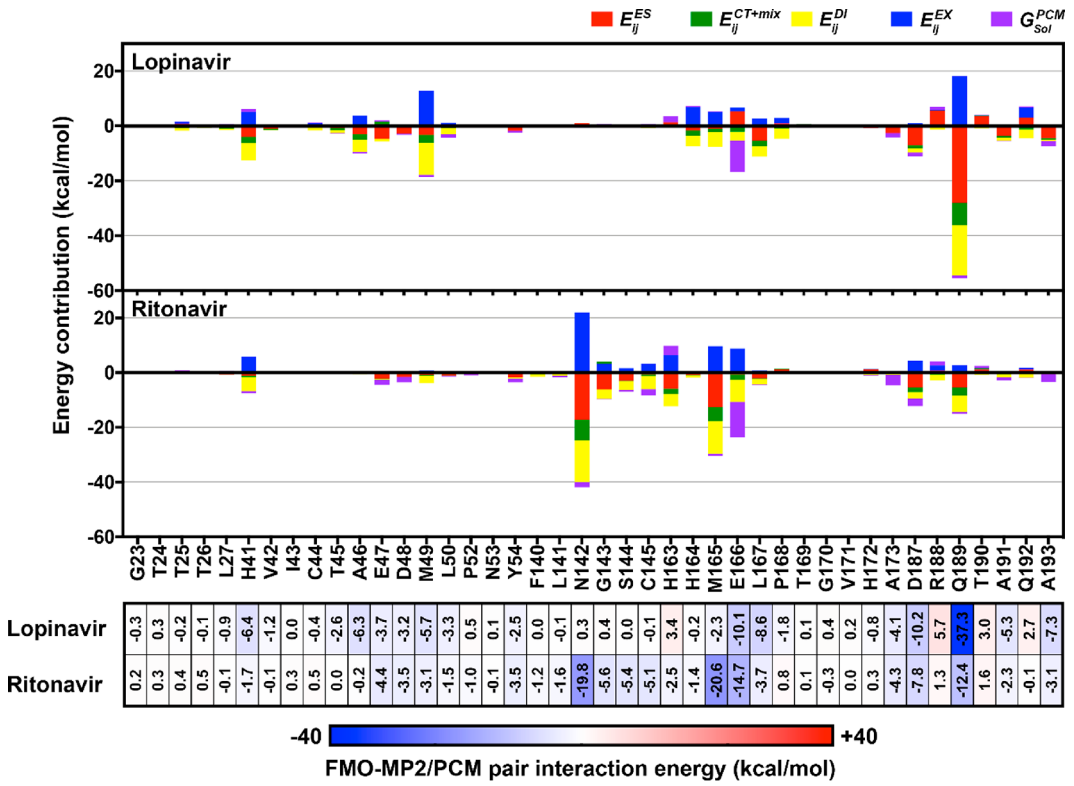

Figure 6. Pair interaction energy decomposition analysis (PIEDA) of lopinavir (top) and ritonavir (bottom) interacting with individual residues in the binding pocket of SARS-CoV-2 $3CL^{pro}$ based on FMO-MP2/PCM/6-31G* calculation.

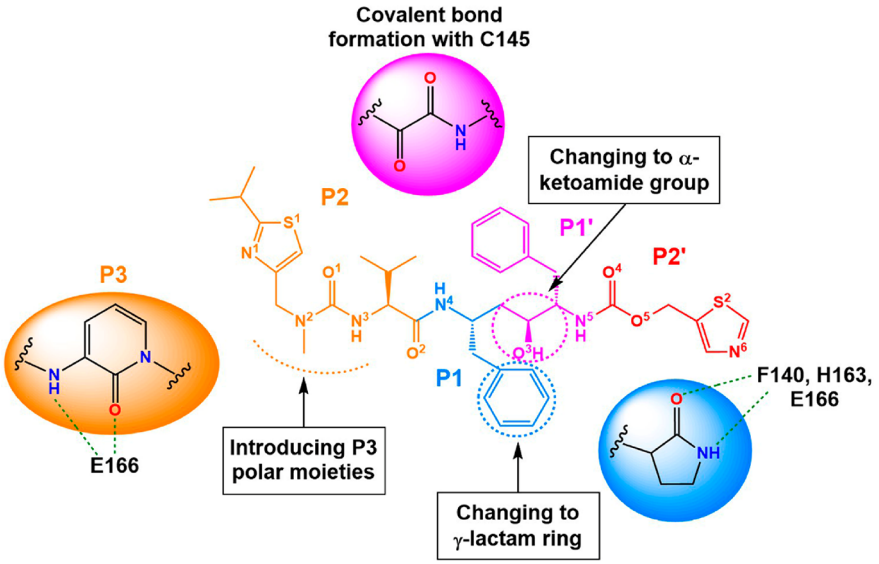

Figure 7. Rational drug design of the SARS-CoV-2 $3CL^{pro}$ inhibitors. Note that the green dashed line indicates H-bond formation.

Predicted Inhibitory Efficiency. The susceptibility of lopinavir and ritonavir to SARS-CoV-2 $3CL^{pro}$ was estimated using the MM/PB(GB)SA approach on 100 snapshots extracted from the last 20 ns of simulation. Note that the MM/PBSA and MM/GBSA results in Table 1 provided a similar trend in the binding free energy predictions.

According to the molecular mechanics (ΔE_{MM}) calculations, we found that van der Waals (vdW) interaction is the main force inducing molecular complexation with SARS-CoV-2 $3CL^{pro}$ of both lopinavir (ΔE_{vdW} of -50.29 ± 0.62 kcal/mol) and ritonavir (-74.09 ± 0.50 kcal/mol) and is ~2−3-fold stronger than the electrostatic attraction (ΔE_{ele} values of -19.68 ± 0.50 and -23.35 ± 0.56 kcal/mol, respectively). This finding was in a good agreement with the ΔE_{MM} results of (i) these two anti-HIV drugs in complex with SARS-CoV $3CL^{pro}$[15] and (ii) darunavir and amprenavir binding to the HIV-1 protease.[43] Taken together with the solvation effect and entropic term, the binding affinity (ΔG_{bind}) of ritonavir with SARS-CoV-2 $3CL^{pro}$ (-14.93 ± 1.83 and -27.78 ± 1.82 kcal/mol taken from the MM/PBSA and MM/GBSA methods, respectively) was relatively higher than that of another drug (-10.89 ± 1.89 and -13.83 ± 1.91 kcal/mol, respectively). The predicted results suggested that

https://dx.doi.org/10.1021/acs.biochem.0c00160
Biochemistry XXXX, XXX, XXX−XXX

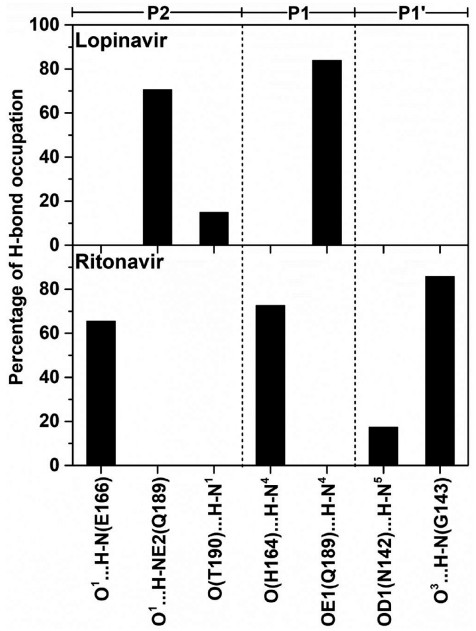

Figure 8. Percentage of H-bond occupation of SARS-CoV-2 3CL^{pro} that contributed to the binding of lopinavir (top) and ritonavir (bottom).

ritonavir may have an ∼1.4−2.0-fold greater inhibitory efficiency than lopinavir on the focused target; however, it should be noted that this drug can clinically also boost the lopinavir efficacy in the fight against COVID-19.

Key Residues for the Repurposed HIV Drug to Combat COVID-19. To evaluate the key residues involved in anti-HIV drug binding at the active site of SARS-CoV-2 3CL^{pro}, the $\Delta G_{bind}^{residue}$ calculation based on the MM/GBSA method was performed. The total energy contribution from each residue associated with drug binding of both complexes is plotted in Figure 3, and the drug orientation in the enzyme active site is illustrated in the right panel, in which the contributing amino acids are colored according to their $\Delta G_{bind}^{residue}$ values. It is important to note that only residues exhibiting an energy stabilization of ≤−1.0 kcal/mol were taken into account.

The obtained results revealed that there were four (M49, M165, P168, and Q189) and nine residues (L27, H41, M49, F140, N142, G143, H164, M165, and E166) that were important for the binding of lopinavir and ritonavir, respectively. The more strongly contributing residues found in the SARS-CoV-2 3CL^{pro}−ritonavir complex were in accordance with the results mentioned above (Figure 2 and Table 1). Similarly, it was reported that the SARS-CoV 3CL^{pro} residues (i) M49 and M165 and (ii) E166 strongly stabilized PJ207, a quinazoline-containing compound, mainly through hydrophobic interaction and H-bond formation, respectively.[44] In line with this finding, our $\Delta G_{bind}^{residue}$ calculation showed that the phenyl ring at the P1 position of lopinavir and the thiazole ring at the P2 position of ritonavir were inserted into the S2 pocket of SARS-CoV-2 3CL^{pro}, forming hydrophobic contacts with residues M49 and M165 (Figure 3), and the O^1 atom of ritonavir was stabilized by the -NH group of E166 via H-bond formation (Figure 6, discussed below). It is of note that only ritonavir could interact with the catalytic residue H41[45] and the oxyanion hole residues N142 and G143[46] ($\Delta G_{bind}^{residue}$ of −1.4 kcal/mol for each residue), suggesting that the molecular structure of ritonavir fitted well within the active site of SARS-CoV-2 3CL^{pro}. The obtained information was supported by the well-aligned structures of ritonavir over the last 20 ns simulation (Figure 4), whereas a large fluctuation of the P2′ site was detected in lopinavir.

In terms of the contribution from the electrostatic (ΔE_{ele} + ΔG_{polar}, black line) and vdW (ΔE_{vdW} + $\Delta G_{nonpolar}$, red line) energies from each residue, it can be seen from Figure 5 that the main energy contribution for stabilizing the HIV-1 protease inhibitors lopinavir and ritonavir was the vdW energy (≲−4.0 kcal/mol), especially for residues M49, M165, and Q189, whereas the electrostatic contribution was observed in the range of approximately −1.0 to 2.0 kcal/mol as related to the ΔE_{MM} calculations (see Table 1). However, there is a common concern about the drawbacks of the molecular mechanics calculations, in particular electronic properties. The FMO-MP2/PCM/6-31G* calculation was additionally performed on the last snapshot of each complex to investigate the protein−drug interactions at the enzyme active site. The advantage of this method is known to include the electron correlation, which trustworthily describes the hydrophobic effect and hydrogen bond interaction between the ligand and individual residue.[40,47,48] Figure 6 highlights that

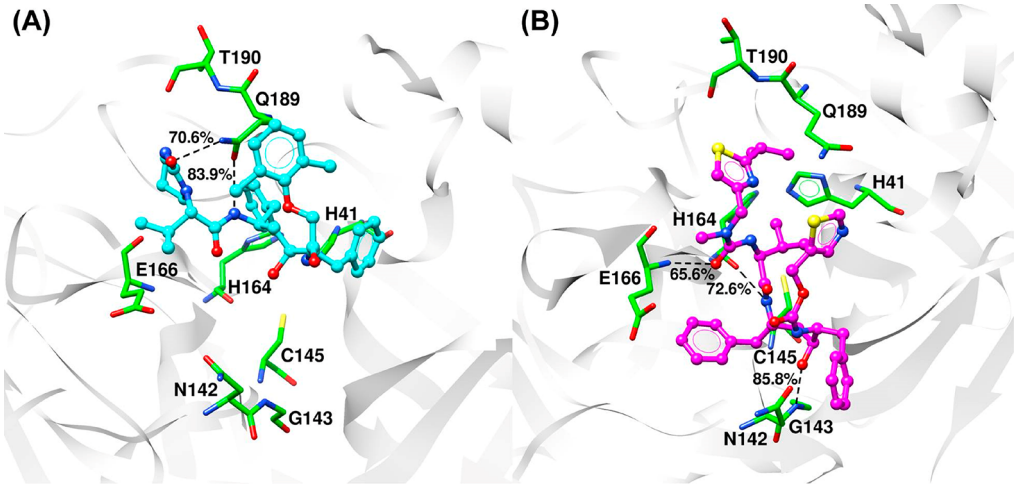

Figure 9. Binding patterns of (A) lopinavir and (B) ritonavir in complex with SARS-CoV-2 3CL^{pro} demonstrated from the last MD snapshot. Black dashed lines represent H-bonds.

https://dx.doi.org/10.1021/acs.biochem.0c00160
Biochemistry XXXX, XXX, XXX−XXX

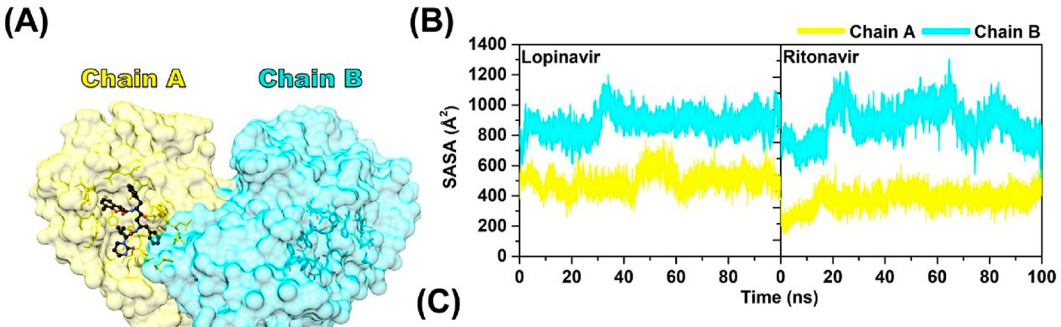

	Average SASA (Å²)	
	Chain A	Chain B
Lopinavir	500.21 ± 67.38	883.81 ± 75.24
Ritonavir	451.60 ± 61.62	918.15 ± 110.03

Figure 10. (A) SARS-CoV-2 3CL^{pro} homodimer, in which chain A with a drug bound and chain B without a drug bound are shown in shades of yellow and blue, respectively. Note that the amino acid residues within 4 Å (stick model) of the ligand (ball and stick representation) were used for SASA calculations. (B) SASA plots along the simulation time of the two studied systems. (C) Average SASAs of lopinavir and ritonavir systems.

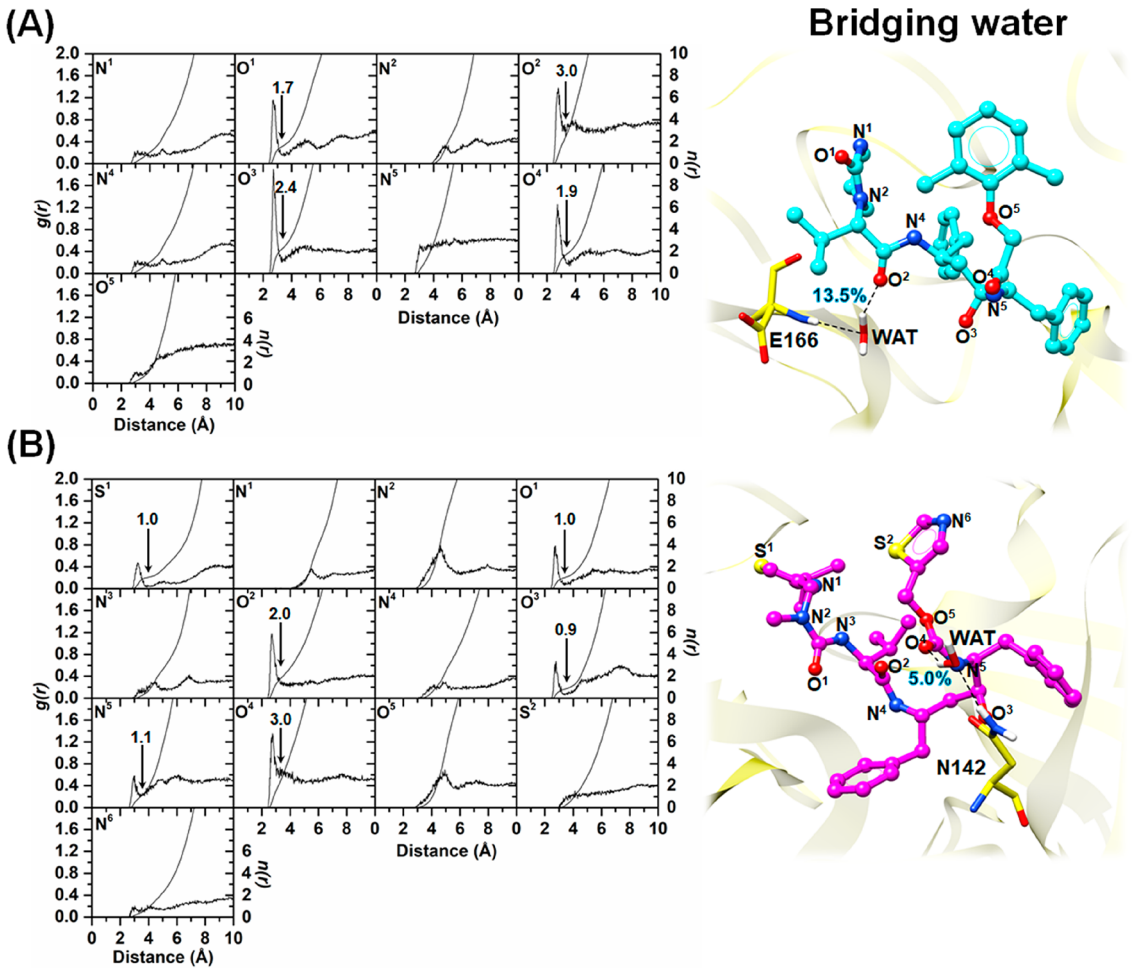

Figure 11. Radial distribution functions, $g(r)$, of the water oxygen atom and integration numbers, $n(r)$, up to the first minimum around the heteroatoms of (A) lopinavir and (B) ritonavir (see Figure 1 for definitions) in complex with SARS-CoV-2 3CL^{pro}. H-Bond water networks of the drug, bridging water, and SARS-CoV-2 3CL^{pro} residue are shown as black dashed lines.

residue Q189 dramatically stabilized lopinavir (−37.3 kcal/mol) mainly through electrostatic, dispersion, and charge transfer contributions (−28.1, −18.3, and −8.1 kcal/mol, respectively), whereas residues H41, A46, M49, E166, L167, L187, A191, and A193 had moderately stabilizing effects with energy values in the range of approximately −5 to −10 kcal/mol via dispersion and/or electrostatic interactions. In contrast, there were four essential amino acids (i.e., N142, M165, E166, and Q189) contributing to

https://dx.doi.org/10.1021/acs.biochem.0c00160
Biochemistry XXXX, XXX, XXX−XXX

ritonavir binding with an energy stabilization of approximately −12 to −20 kcal/mol, whereas residues G143, S144, C145, and D187 showed less energy stabilization of approximately −5 to −7 kcal/mol, most likely through dispersion and electrostatic interactions, except for residue E166, for which the impact of the solvation effect was predominantly found on the two drugs binding to SARS-CoV-2 3CL^{pro}.

As compared to the recently reported potent α-ketoamide inhibitor (13b) bound to SARS-CoV-2 3CL^{pro},[49] the anti-HIV drugs lopinavir and ritonavir lack (i) the P3 moiety, (ii) an α-ketoamide group located between positions P1 and P1′, and (iii) polar moieties on the phenyl ring in the P1 region. However, the phenyl ring at the P1′ site of both HIV-1 protease inhibitors and 13b remains the same, and the P2 (larger and more hydrophilic than 13b) and P2′ (found only in HIV-1 protease inhibitors) regions of lopinavir and ritonavir strongly interacted with SARS-CoV-2 3CL^{pro} at the S2 and S2′ pockets, respectively (Figure 3). Accordingly, on the basis of this evidence, we proposed a rational design of novel protease inhibitor(s) derived from lopinavir and ritonavir to enhance the binding efficiency with SARS-CoV-2 3CL^{pro} as follows: (i) changing the phenyl ring in the P1 region to the γ-lactam ring to increase the extent of H-bond formation with residues F140, H163, and E166, (ii) introducing P3 polar moieties (e.g., pyridone ring) to form H-bonds with the negatively charged E166, and (iii) adding the reactive α-ketoamide group located between positions P1 and P1′ to covalently bond with the catalytic residue C145, as depicted in Figure 7.

Protein−Drug Hydrogen Bonding. Although the protein−drug interactions were primarily contributed by the vdW interactions, the formation of H-bonds between both anti-HIV drugs and their surrounding residues in the active site of SARS-CoV-2 3CL^{pro} could be an important factor in the inhibition of this targeted enzyme. To monitor such interaction, the percentages of H-bond occupations are plotted in Figure 8, whereas the representative structures determined from the last MD snapshot are depicted in Figure 9. As expected, H-bond formation (three to four H-bonds) between the drugs and the surrounding residues inside the active site of SARS-CoV-2 3CL^{pro} was observed. In the case of lopinavir, there were three H-bonds: (i) O^1(P2 site)···H−NE2(Q189) at 70.6%, (ii) O(T190)···H−N^1(P2 site) at 14.8%, and (iii) OE1(Q189)···H−N^4(P1 site) at 83.9%. Meanwhile, four H-bonds were detected in the ritonavir complex: (i) O^1(P2 site)···H−N(E166) at 65.6%, (ii) O(H164)···H−N^4(P1 site) at 72.6%, (iii) OD1(N142)···H−N^5(P1′ site) at 17.3%, and (iv) O^3(P1′ site)···H−N(G143) at 85.6%. It can be noticed that the importance of residues E166 and Q189 also agreed well with the reported binding of such HIV-1 protease inhibitors to SARS-CoV.[15] Notably, ritonavir showed a slightly higher level of H-bond formation with 3CL^{pro}, and its P1′ site was stabilized by the oxyanion hole residues N142 and G143.

Solvent Accessibility in the 3CL^{pro} Active Site. As the active site of SARS-CoV-2 3CL^{pro} is located near the solvent-exposed area, water molecules might play a role in stabilizing protein−ligand interactions. To characterize the effect of water accessibility at the 3CL^{pro} active site, the solvent-accessible surface area (SASA) (Figure 10) calculations were performed on the residues within 4 Å of each anti-HIV drug. Moreover, the radial distribution function (RDF) (Figure 11) of water oxygens toward all heteroatoms of lopinavir and ritonavir was used to verify the number of water molecules approaching the ligands.

Our complex model of the SARS-CoV-2 3CL^{pro} homodimer contained the anti-HIV drugs binding only to protomer A. It can be seen from Figure 10 that the SASAs for protomer B (blue) were 883.81 ± 75.24 and 918.15 ± 110.03 Å^2 for the lopinavir and ritonavir systems, respectively. Upon molecular complexation in protomer A (yellow), the SASAs of both lopinavir (500.21 ± 67.38 Å^2) and ritonavir (451.60 ± 61.62 Å^2) systems dramatically decreased in a manner similar to those of other studies.[50−52] By considering the RDF results, we found that the first peak at ∼3 Å of the lopinavir system (up to ∼2) was slightly higher than that of the ritonavir system (up to ∼1.4), indicating that accessible water molecules were more pronounced in the SARS-CoV-2 3CL^{pro}−lopinavir complex. As the H-bond water network, protein···water···drug, also plays a role in stabilizing the protein−ligand complex,[53] we further investigated the H-bond water bridges around the heteroatoms of both ligands using the same structural criteria of H-bonds described elsewhere. The obtained results demonstrated that there was only one bridging water coordinating with (i) lopinavir (O^2) and E166 as well as (ii) ritonavir (O^4) and N142 with a very low percentage of occupancy (∼5−13%), suggesting that the bridging water did not make a significant contribution to mediating the H-bond network of protein−ligand binding.

CONCLUSIONS

In this work, the binding pattern and susceptibility of the two HIV-1 protease inhibitors lopinavir and ritonavir in complex with SARS-CoV-2 3CL^{pro} were fully revealed by all-atom MD simulations, binding free energy estimation, and PIEDA based on the MM/PB(GB)SA and FMO-MP2/PCM/6-31G* calculations, respectively. According to ΔG_{bind} prediction, the susceptibility against SARS-CoV-2 3CL^{pro} of ritonavir was somewhat higher than that of lopinavir, supported by energy stabilization from individual residues that resulted from both methods: (i) M49, M165, P168, and Q189 from MM/GBSA for lopinavir and L27, H41, M49, F140, N142, G143, H164, M165, and E166 from MM/GBSA for ritonavir and (ii) H41, A46, M49, E166, L167, L187, Q189, A191, and A193 from FMO-MP2/PCM/6-31G* for lopinavir and N142, G143, S144, C145, M165, E166, D187, and Q189 from FMO-MP2/PCM/6-31G* for ritonavir. In addition, the oxyanion hole residues N142 and G143 were found to interact with ritonavir via hydrogen bonds. From the FMO-MP2/PCM/6-31G* data, the electrostatics, dispersion, and charge transfer were considered as the important interactions for drug binding. The obtained results demonstrated how repurposed anti-HIV drugs could be used to combat COVID-19 and how fundamental knowledge at the atomic level could also be helpful for the further design or development of more specific inhibitors in treating human coronaviruses.

ASSOCIATED CONTENT

Supporting Information

The Supporting Information is available free of charge at https://pubs.acs.org/doi/10.1021/acs.biochem.0c00160.

Amino acid sequences and structural comparison (PDF)

AUTHOR INFORMATION

Corresponding Authors

Thanyada Rungrotmongkol − *Structural and Computational Biology Research Unit, Department of Biochemistry, Faculty of Science and Program in Bioinformatics and Computational Biology, Graduate School, Chulalongkorn University, Bangkok*

https://dx.doi.org/10.1021/acs.biochem.0c00160
Biochemistry XXXX, XXX, XXX−XXX

10330, Thailand; orcid.org/0000-0002-7402-3235; Phone: +66 2 218-5426; Email: thanyada.r@chula.ac.th; Fax: +66 2 218-5418

Supot Hannongbua − *Center of Excellence in Computational Chemistry (CECC), Department of Chemistry, Faculty of Science, Chulalongkorn University, Bangkok 10330, Thailand*; Phone: +66 2 218-7602; Email: supot.h@chula.ac.th; Fax: +66 2 218-7603

Authors

Bodee Nutho − *Center of Excellence in Computational Chemistry (CECC), Department of Chemistry, Faculty of Science, Chulalongkorn University, Bangkok 10330, Thailand*

Panupong Mahalapbutr − *Structural and Computational Biology Research Unit, Department of Biochemistry, Faculty of Science, Chulalongkorn University, Bangkok 10330, Thailand*

Kowit Hengphasatporn − *Center for Computational Sciences, University of Tsukuba, Tsukuba, Ibaraki 305-8577, Japan*

Nawanwat Chainuwong Pattaranggoon − *Program in Bioinformatics and Computational Biology, Graduate School, Chulalongkorn University, Bangkok 10330, Thailand*

Nattapon Simanon − *Program in Bioinformatics and Computational Biology, Graduate School, Chulalongkorn University, Bangkok 10330, Thailand*

Yasuteru Shigeta − *Center for Computational Sciences, University of Tsukuba, Tsukuba, Ibaraki 305-8577, Japan;* orcid.org/0000-0002-3219-6007

Complete contact information is available at: https://pubs.acs.org/10.1021/acs.biochem.0c00160

Author Contributions

⊥B.N. and P.M. contributed equally to this work.

Funding

The Second Century Fund (C2F), Chulalongkorn University (CU) is acknowledged for B.N. and P.M. (postdoctoral fellowship) and N.C.P. (Ph.D. scholarship). NSTDA Supercomputer Center (ThaiSC) is acknowledged for facilities and computing resources.

Notes

The authors declare no competing financial interest.

REFERENCES

(1) Chen, N., Zhou, M., Dong, X., Qu, J., Gong, F., Han, Y., Qiu, Y., Wang, J., Liu, Y., Wei, Y., Xia, J., Yu, T., Zhang, X., and Zhang, L. (2020) Epidemiological and clinical characteristics of 99 cases of 2019 novel coronavirus pneumonia in Wuhan, China: a descriptive study. *Lancet 395* (10223), 507−513.

(2) Paraskevis, D., Kostaki, E. G., Magiorkinis, G., Panayiotakopoulos, G., Sourvinos, G., and Tsiodras, S. (2020) Full-genome evolutionary analysis of the novel corona virus (2019-nCoV) rejects the hypothesis of emergence as a result of a recent recombination event. *Infect., Genet. Evol. 79*, 104212.

(3) Lu, R., Zhao, X., Li, J., Niu, P., Yang, B., Wu, H., Wang, W., Song, H., Huang, B., Zhu, N., Bi, Y., Ma, X., Zhan, F., Wang, L., Hu, T., Zhou, H., Hu, Z., Zhou, W., Zhao, L., Chen, J., Meng, Y., Wang, J., Lin, Y., Yuan, J., Xie, Z., Ma, J., Liu, W. J., Wang, D., Xu, W., Holmes, E. C., Gao, G. F., Wu, G., Chen, W., Shi, W., and Tan, W. (2020) Genomic characterisation and epidemiology of 2019 novel coronavirus: implications for virus origins and receptor binding. *Lancet 395*, 565.

(4) Brian, D. A., and Baric, R. S. (2005) Coronavirus genome structure and replication. *Curr. Top. Microbiol. Immunol. 287*, 1−30.

(5) Zhang, X. M., Herbst, W., Kousoulas, K. G., and Storz, J. (1994) Biological and genetic characterization of a hemagglutinating coronavirus isolated from a diarrhoeic child. *J. Med. Virol. 44* (2), 152−161.

(6) Yang, H., Bartlam, M., and Rao, Z. (2006) Drug design targeting the main protease, the Achilles' heel of coronaviruses. *Curr. Pharm. Des. 12* (35), 4573−4590.

(7) Huang, C., Wang, Y., Li, X., Ren, L., Zhao, J., Hu, Y., Zhang, L., Fan, G., Xu, J., Gu, X., Cheng, Z., Yu, T., Xia, J., Wei, Y., Wu, W., Xie, X., Yin, W., Li, H., Liu, M., Xiao, Y., Gao, H., Guo, L., Xie, J., Wang, G., Jiang, R., Gao, Z., Jin, Q., Wang, J., and Cao, B. (2020) Clinical features of patients infected with 2019 novel coronavirus in Wuhan, China. *Lancet 395*, 497.

(8) Xu, R. H., He, J. F., Evans, M. R., Peng, G. W., Field, H. E., Yu, D. W., Lee, C. K., Luo, H. M., Lin, W. S., Lin, P., Li, L. H., Liang, W. J., Lin, J. Y., and Schnur, A. (2004) Epidemiologic clues to SARS origin in China. *Emerging Infect. Dis. 10* (6), 1030−1037.

(9) de Groot, R. J., Baker, S. C., Baric, R. S., Brown, C. S., Drosten, C., Enjuanes, L., Fouchier, R. A. M., Galiano, M., Gorbalenya, A. E., Memish, Z. A., Perlman, S., Poon, L. L. M., Snijder, E. J., Stephens, G. M., Woo, P. C. Y., Zaki, A. M., Zambon, M., and Ziebuhr, J. (2013) Middle east respiratory syndrome coronavirus (MERS-CoV): Announcement of the coronavirus study group. *J. Virol. 87* (14), 7790−7792.

(10) Chan, J. F. W., Yuan, S., Kok, K. H., Chu, K. K. W., Yang, H., Xing, J., Liu, F., Yip, J., Poon, C. C. Y., Tsoi, R. W. S., Lo, H. W., Chan, S. K. F., Poon, K. H., Chan, V. K. M., Ip, W. M., Cai, J. D., Cheng, J. P., Chen, V. C. C., Hui, C. K.-M., To, K. K.-W., and Yuen, K. Y. (2020) A familial cluster of pneumonia associated with the 2019 novel coronavirus indicating person-to-person transmission: a study of a family cluster. *Lancet 395*, 514.

(11) Su, S., Wong, G., Shi, W., Liu, J., Lai, A. C. K., Zhou, J., Liu, W., Bi, Y., and Gao, G. F. (2016) Epidemiology, Genetic Recombination, and Pathogenesis of Coronaviruses. *Trends Microbiol. 24* (6), 490−502.

(12) De Clercq, E., and Li, G. (2016) Approved antiviral drugs over the past 50 years. *Clin. Microbiol. Rev. 29* (3), 695−747.

(13) Kaplan, S. S., and Hicks, C. B. (2005) Lopinavir/ritonavir in the treatment of human immunodeficiency virus infection. *Expert Opin. Pharmacother. 6* (9), 1573−1585.

(14) Chu, C. M., Cheng, V. C. C., Hung, I. F. N., Wong, M. M. L., Chan, K. H., Chan, K. S., Kao, R. Y. T., Poon, L. L. M., Wong, C. L. P., Guan, Y., Peiris, J. S. M., and Yuen, K. Y. (2004) Role of lopinavir/ritonavir in the treatment of SARS: Initial virological and clinical findings. *Thorax 59* (3), 252−256.

(15) Nukoolkarn, V., Lee, V. S., Malaisree, M., Aruksakulwong, O., and Hannongbua, S. (2008) Molecular dynamic simulations analysis of ritronavir and lopinavir as SARS-CoV 3CLpro inhibitors. *J. Theor. Biol. 254* (4), 861−867.

(16) Liu, X., and Wang, X.-J. (2020) Potential inhibitors against 2019-nCoV coronavirus M protease from clinically approved medicines. *J. Genet. Genomics 47*, 119.

(17) Zumla, A., Chan, J. F. W., Azhar, E. I., Hui, D. S. C., and Yuen, K. Y. (2016) Coronaviruses-drug discovery and therapeutic options. *Nat. Rev. Drug Discovery 15* (5), 327−347.

(18) Anand, K., Ziebuhr, J., Wadhwani, P., Mesters, J. R., and Hilgenfeld, R. (2003) Coronavirus main proteinase (3CLpro) Structure: Basis for design of anti-SARS drugs. *Science 300* (5626), 1763−1767.

(19) Arabi, Y. M., Alothman, A., Balkhy, H. H., Al-Dawood, A., AlJohani, S., Al Harbi, S., Kojan, S., Al Jeraisy, M., Deeb, A. M., Assiri, A. M., Al-Hameed, F., AlSaedi, A., Mandourah, Y., Almekhlafi, G. A., Sherbeeni, N. M., Elzein, F. E., Memon, J., Taha, Y., Almotairi, A., Maghrabi, K. A., Qushmaq, I., Al Bshabshe, A., Kharaba, A., Shalhoub, S., Jose, J., Fowler, R. A., Hayden, F. G., Hussein, M. A., Martin, G. S., Schoenfeld, D. A., Walmsley, S. L., Carson, S., Harbi, S. A., Jeraisy, M. A., Muhaidib, M. A., Musharaf, S., Anizi, H. A., Dael, R., AlMazroa, M., Asiri, A., Memish, Z. A., Ghazal, S. S., Alfaraj, S. H., Harthy, A. A., Sulaiman, M. A., Mady, A., Ahmad, A., Ghaleb, A. A., Muhammed, R., Samirrai, S. A., Awad, S., Cabal, R. C., Onazi, B. A., Aljuhani, M., Vince, M., Enani, M. A., Alqurashi, A., Alenezi, F., Alkhani, N., Thaqafi, A., Oraabi, O. A., Rifai, J., Elsamadisi, P., Medhat, S. H., Basher, S. A.,

Abduldhaher, M., Bajhamoum, W., Alahsa, S. S., Bashir, S., Al-Dossary, I., Al-Muhainy Dammam, B., Khobar, S. S. A., Alshahrani, M. S., Al Jabri, A., Farid, M., Alaidarous, A., Alseraihi, W., Shahada, H., and Taif, J. S. (2018) Treatment of Middle East Respiratory Syndrome with a combination of lopinavir-ritonavir and interferon-β1b (MIRACLE trial): Study protocol for a randomized controlled trial. *Trials 19*, n/a.

(20) Zeldin, R. K., and Petruschke, R. A. (2003) Pharmacological and therapeutic properties of ritonavir-boosted protease inhibitor therapy in HIV-infected patients. *J. Antimicrob. Chemother. 53* (1), 4−9.

(21) Jin, Z., Du, X., Xu, Y., Deng, Y., Liu, M., Zhao, Y., Zhang, B., Li, X., Zhang, L., Peng, C., Duan, Y., Yu, J., Wang, L., Yang, K., Liu, F., Jiang, R., Yang, X., You, T., Liu, X., Yang, X., Bai, F., Liu, H., Liu, X., Guddat, L. W., Xu, W., Xiao, G., Qin, C., Shi, Z., Jiang, H., Rao, Z., and Yang, H. (2020) Structure of M^{pro} from COVID-19 virus and discovery of its inhibitors. *Nature*, DOI: 10.1038/s41586-020-2223-y.

(22) Anandakrishnan, R., Aguilar, B., and Onufriev, A. V. (2012) H++ 3.0: Automating pK prediction and the preparation of biomolecular structures for atomistic molecular modeling and simulations. *Nucleic Acids Res. 40* (W1), W537−W541.

(23) Otto, H. H., and Schirmeister, T. (1997) Cysteine proteases and their inhibitors. *Chem. Rev. 97* (1), 133−171.

(24) Sterling, T., and Irwin, J. J. (2015) ZINC 15 - Ligand Discovery for Everyone. *J. Chem. Inf. Model. 55* (11), 2324−2337.

(25) Frisch, M. J., Trucks, G. W., Schlegel, H. B., Scuseria, G. E., Robb, M. A., Cheeseman, J. R., Scalmani, G., Barone, V., Mennucci, B., Petersson, G. A., Nakatsuji, H., Caricato, M., Li, X., Hratchian, H. P., Izmaylov, A. F., Bloino, J., Zheng, G., Sonnenberg, J. L., Hada, M., Ehara, M., Toyota, K., Fukuda, R., Hasegawa, J., Ishida, M., Nakajima, T., Honda, Y., Kitao, O., Nakai, H., Vreven, T., Montgomery, J. A., Jr., Peralta, J. E., Ogliaro, F., Bearpark, M. J., Heyd, J., Brothers, E. N., Kudin, K. N., Staroverov, V. N., Kobayashi, R., Normand, J., Raghavachari, K., Rendell, A. P., Burant, J. C., Iyengar, S. S., Tomasi, J., Cossi, M., Rega, N., Millam, N. J., Klene, M., Knox, J. E., Cross, J. B., Bakken, V., Adamo, C., Jaramillo, J., Gomperts, R., Stratmann, R. E., Yazyev, O., Austin, A. J., Cammi, R., Pomelli, C., Ochterski, J. W., Martin, R. L., Morokuma, K., Zakrzewski, V. G., Voth, G. A., Salvador, P., Dannenberg, J. J., Dapprich, S., Daniels, A. D., Farkas, Ö., Foresman, J. B., Ortiz, J. V., Cioslowski, J., and Fox, D. J. (2009) *Gaussian 09*, Gaussian, Inc., Wallingford, CT.

(26) Maier, J. A., Martinez, C., Kasavajhala, K., Wickstrom, L., Hauser, K. E., and Simmerling, C. (2015) ff14SB: Improving the Accuracy of Protein Side Chain and Backbone Parameters from ff99SB. *J. Chem. Theory Comput. 11* (8), 3696−3713.

(27) Wang, J., Wolf, R. M., Caldwell, J. W., Kollman, P. A., and Case, D. A. (2004) Development and testing of a general Amber force field. *J. Comput. Chem. 25* (9), 1157−1174.

(28) Jorgensen, W. L., Chandrasekhar, J., Madura, J. D., Impey, R. W., and Klein, M. L. (1983) Comparison of simple potential functions for simulating liquid water. *J. Chem. Phys. 79* (2), 926−935.

(29) Meeprasert, A., Hannongbua, S., and Rungrotmongkol, T. (2014) Key binding and susceptibility of NS3/4A serine protease inhibitors against hepatitis C virus. *J. Chem. Inf. Model. 54* (4), 1208−1217.

(30) Mahalapbutr, P., Wonganan, P., Chavasiri, W., and Rungrotmongkol, T. (2019) Butoxy Mansonone G Inhibits STAT3 and Akt Signaling Pathways in Non-Small Cell Lung Cancers: Combined Experimental and Theoretical Investigations. *Cancers 11* (4), 437.

(31) Nutho, B., and Rungrotmongkol, T. (2019) Binding recognition of substrates in NS2B/NS3 serine protease of Zika virus revealed by molecular dynamics simulations. *J. Mol. Graphics Modell. 92*, 227−235.

(32) Kammarabutr, J., Mahalapbutr, P., Nutho, B., Kungwan, N., and Rungrotmongkol, T. (2019) Low susceptibility of asunaprevir towards R155K and D168A point mutations in HCV NS3/4A protease: A molecular dynamics simulation. *J. Mol. Graphics Modell. 89*, 122−130.

(33) Darden, T., York, D., and Pedersen, L. (1993) Particle mesh Ewald: An N·log(N) method for Ewald sums in large systems. *The. J. Chem. Phys. 98* (12), 10089−10092.

(34) Ryckaert, J. P., Ciccotti, G., and Berendsen, H. J. C. (1977) Numerical integration of the cartesian equations of motion of a system with constraints: molecular dynamics of n-alkanes. *J. Comput. Phys. 23* (3), 327−341.

(35) Uberuaga, B. P., Anghel, M., and Voter, A. F. (2004) Synchronization of trajectories in canonical molecular-dynamics simulations: Observation, explanation, and exploitation. *J. Chem. Phys. 120* (14), 6363−6374.

(36) Berendsen, H. J. C., Postma, J. P. M., Van Gunsteren, W. F., Dinola, A., and Haak, J. R. (1984) Molecular dynamics with coupling to an external bath. *J. Chem. Phys. 81* (8), 3684−3690.

(37) Roe, D. R., and Cheatham, T. E. (2013) PTRAJ and CPPTRAJ: Software for processing and analysis of molecular dynamics trajectory data. *J. Chem. Theory Comput. 9* (7), 3084−3095.

(38) Miller, B. R., III, McGee, T. D., Swails, J. M., Homeyer, N., Gohlke, H., and Roitberg, A. E. (2012) MMPBSA.py: An efficient program for end-state free energy calculations. *J. Chem. Theory Comput. 8* (9), 3314−3321.

(39) Feyereisen, M., Fitzgerald, G., and Komornicki, A. (1993) Use of approximate integrals in ab initio theory. An application in MP2 energy calculations. *Chem. Phys. Lett. 208* (5−6), 359−363.

(40) Kitaura, K., Sugiki, S. I., Nakano, T., Komeiji, Y., and Uebayasi, M. (2001) Fragment molecular orbital method: Analytical energy gradients. *Chem. Phys. Lett. 336* (1−2), 163−170.

(41) Fedorov, D. G., and Kitaura, K. (2007) Pair interaction energy decomposition analysis. *J. Comput. Chem. 28* (1), 222−237.

(42) Hengphasatporn, K., Garon, A., Wolschann, P., Langer, T., Yasuteru, S., Huynh, T. N. T., Chavasiri, W., Saelee, T., Boonyasuppayakorn, S., and Rungrotmongkol, T. (2020) Multiple virtual screening strategies for the discovery of novel compounds active against dengue virus: A hit identification study. *Sci. Pharm. 88* (1), 2.

(43) Chen, J., Liang, Z., Wang, W., Yi, C., Zhang, S., and Zhang, Q. (2015) Revealing Origin of Decrease in Potency of Darunavir and Amprenavir against HIV-2 relative to HIV-1 Protease by Molecular Dynamics Simulations. *Sci. Rep. 4* (1), 6872.

(44) Mukherjee, P., Shah, F., Desai, P., and Avery, M. (2011) Inhibitors of SARS-3CLpro: virtual screening, biological evaluation, and molecular dynamics simulation studies. *J. Chem. Inf. Model. 51* (6), 1376−1392.

(45) Shi, J., Han, N., Lim, L., Lua, S., Sivaraman, J., Wang, L., Mu, Y., and Song, J. (2011) Dynamically-driven inactivation of the catalytic machinery of the SARS 3C-like protease by the N214A mutation on the extra domain. *PLoS Comput. Biol. 7* (2), e1001084−e1001084.

(46) Verschueren, K. H. G., Pumpor, K., Anemüller, S., Chen, S., Mesters, J. R., and Hilgenfeld, R. (2008) A structural view of the inactivation of the SARS coronavirus main proteinase by benzotriazole esters. *Chem. Biol. 15* (6), 597−606.

(47) Maruyama, K., Sheng, Y., Watanabe, H., Fukuzawa, K., and Tanaka, S. (2018) Application of singular value decomposition to the inter-fragment interaction energy analysis for ligand screening. *Comput. Theor. Chem. 1132*, 23−34.

(48) Choi, J., Kim, H. J., Jin, X., Lim, H., Kim, S., Roh, I. S., Kang, H. E., No, K. T., and Sohn, H. J. (2018) Application of the fragment molecular orbital method to discover novel natural products for prion disease. *Sci. Rep. 8* (1), 13063.

(49) Zhang, L., Lin, D., Sun, X., Curth, U., Drosten, C., Sauerhering, L., Becker, S., Rox, K., and Hilgenfeld, R. (2020) Crystal structure of SARS-CoV-2 main protease provides a basis for design of improved α-ketoamide inhibitors. *Science*, eabb3405.

(50) Shahbaaz, M., Amir, M., Rahman, S., Mustafa Hasan, G., Dohare, R., Bisetty, K., Ahmad, F., Kim, J., and Hassan, M. I. (2018) Structural insights into Rab21 GTPase activation mechanism by molecular dynamics simulations. *Mol. Simul. 44* (3), 179−189.

(51) Mahalapbutr, P., Darai, N., Panman, W., Opasmahakul, A., Kungwan, N., Hannongbua, S., and Rungrotmongkol, T. (2019) Atomistic mechanisms underlying the activation of the G protein-coupled sweet receptor heterodimer by sugar alcohol recognition. *Sci. Rep. 9* (1), 10205.

https://dx.doi.org/10.1021/acs.biochem.0c00160
Biochemistry XXXX, XXX, XXX−XXX

(52) Cao, K., Li, N., Wang, H., Cao, X., He, J., Zhang, B., He, Q.-Y., Zhang, G., and Sun, X. (2018) Two zinc-binding domains in the transporter AdcA from Streptococcus pyogenes facilitate high-affinity binding and fast transport of zinc. *J. Biol. Chem. 293* (16), 6075−6089.
(53) Duan, L., Feng, G., Wang, X., Wang, L., and Zhang, Q. (2017) Effect of electrostatic polarization and bridging water on CDK2-ligand binding affinities calculated using a highly efficient interaction entropy method. *Phys. Chem. Chem. Phys. 19* (15), 10140−10152.

https://dx.doi.org/10.1021/acs.biochem.0c00160
Biochemistry XXXX, XXX, XXX−XXX